

DRAFT: EXPERIMENTAL INVESTIGATION OF CONTOURED ENDWALL AND LEADING EDGE FILLET CONFIGURATIONS AND COMPUTATIONAL EVALUATION

Özhan H. Turgut*

Turbomachinery Aero-Heat Transfer Laboratory
 Department Aerospace Engineering
 The Pennsylvania State University
 University Park, Pennsylvania 16802
 Email: oht101@psu.edu

Cengiz Camci†

Turbomachinery Aero-Heat Transfer Laboratory
 Department Aerospace Engineering
 The Pennsylvania State University
 University Park, Pennsylvania 16802
 Email: cxc11@psu.edu

ABSTRACT

Secondary flow minimization is a crucial problem in a turbine passage. In the present paper, three different ways are employed to reduce the secondary flow related total pressure loss. These are nonaxisymmetric endwall contouring, leading edge (LE) fillet, and the combination of these two approaches. Experimental investigation and computational assessment are applied for the performance calculations. The experiments are carried out in an annular Axial Flow Turbine Research Facility (AFTRF) having a diameter of 91.66cm. For the experimental measurement comparison, a reference Flat Insert is installed in the nozzle guide vane (NGV) passage. It has a constant thickness with cylindrical surface and is manufactured by stereolithography (SLA) method. Also, Flat Insert has a backward facing step at the NGV exit, and the effect of this step is analyzed computationally. Four different LE fillets are designed, and they are attached to both cylindrical Flat Insert and the contoured endwall. Total pressure measurements are taken at rotor inlet plane with Kiel probe. The probe traversing is completed with one vane pitch and from 8% to 38% span. For one of the designs, area-averaged loss is reduced by 15.06%. The simulation estimated this reduction as 6.95%. Computational evaluation is also performed at the NGV exit plane. The most effective design reduced the mass-averaged loss by 1.84% on the whole passage. The computational study did not include the rim seal flow between the vane and rotor domain and also rotor simulation was absent. The

difference between the measurements and the simulation comes from these two important effects.

NOMENCLATURE

c Midspan axial chord length of nozzle guide vane.

c_{hub} Hub axial chord length of nozzle guide vane.

C_{P_t} Total pressure coefficient; $(P_0 - P_1)/(0.5 \rho V_1^2)$.

P_0 Total pressure.

Re_{θ_l} Momentum-thickness Reynolds number.

V Velocity magnitude.

x Axial distance from nozzle guide vane leading edge.

y^+ Non-dimensional wall coordinate; $\frac{\sqrt{\tau_w}/\rho}{V} y_p$.

y_p First grid height off the wall.

Greek

γ Intermittency.

ν Kinematic viscosity.

ρ Density.

τ_w Wall shear stress.

ω Turbulent frequency.

Subscripts

1 One axial chord upstream of nozzle guide vane leading edge.

2 Nozzle guide vane exit plane, $x/c = 1.025$.

Abbreviations

N Turbine nozzle guide vane.

R Turbine blade.

SST Shear stress transport.

TKE Turbulence kinetic energy.

*Graduate Research Assistant, ASME Student Member

†Professor of Aerospace Engineering, ASME Fellow

INTRODUCTION

Sharma and Butler [1] states that the endwall losses represent 30-50% of the total pressure loss. Also, according to a very explanatory paper by Denton [2], $\frac{1}{3}$ of the total loss in a turbine passage is governed by endwall losses. Two important parameters play a significant role in the production of endwall losses within and outside of the turbine blade: thickness of the inlet boundary layer and the amount of turning of the blade. When the incoming boundary layer sees a blunt object, the particles outside the boundary layer tends to turn onto low momentum particles closer to the endwall. As a result, a roll-up vortex occurs in front of the leading edge, and this vortex separates into two parts, known as the horseshoe vortex. The strong cross-passage pressure gradient causes the pressure side leg of horseshoe vortex to move towards the suction surface of the adjacent blade. This leg merges with the passage vortex and later on suction side leg wraps itself around this passage vortex. The strong cross-flow within the blade passage, from pressure side to suction side, feeds this flow structure, enhances it and lifts it off the endwall surface. It is clear from this secondary flow model that special attention should be given to the formation of the horseshoe vortex and the crossflow occurrence within the passage.

Aerodynamic losses related to this horseshoe vortex can be minimized using a leading edge fillet, which fills the intersection of the nozzle guide vane (NGV) and the hub endwall. It forms a smooth transition from the NGV leading edge to the endwall surface. These leading edge fillets are also useful in heat transfer point of view. Minimizing the vortices results in lower mixing of the fluid near midspan and near endwall. Therefore, many researchers have been studying the effects of these leading edge fillets on turbine NGV's.

One of the earliest studies of using a leading edge modification in turbine cascades was performed by Sauer et al. [3]. The aim of the study was to reduce the secondary flow losses. The methodology was to design a bulb like geometry at the leading edge endwall junction such that the suction side leg of the horseshoe vortex became strengthened. Then the interaction of this strong suction side leg with the counterrotating pressure side leg (which merges with the passage vortex) would keep passage vortex away from the profile boundary layer resulting in a reduced endwall losses. They tested three different bulb like geometries at the intersection of the leading edge and the endwall. Unlike a fillet, this bulb geometry was orthogonal to the endwall at the intersection line. The presented results showed a 47% decrease in endwall loss (measured loss subtracted the inlet boundary layer loss and the profile loss). This was achieved by using a nonsymmetric bulb geometry. The computational results did not calculate the absolute values exactly.

Another leading edge fillet experiment was conducted by Zess and Thole [4]. They tried to eliminate the horseshoe vortex by using a fillet of having one boundary layer thickness in height and two boundary layer thickness in length. The most efficient

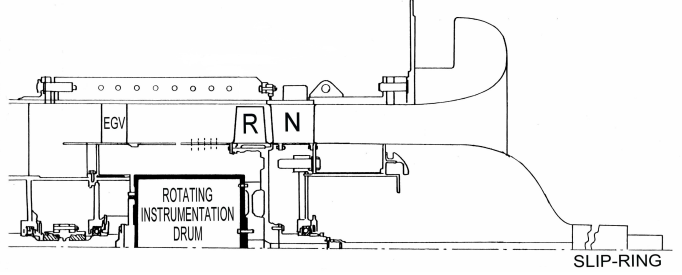
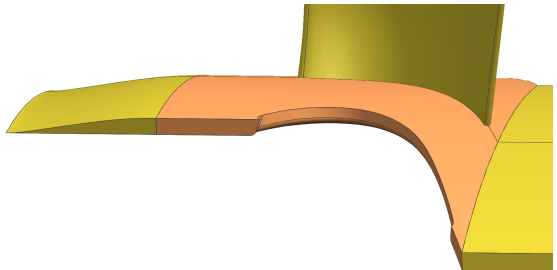
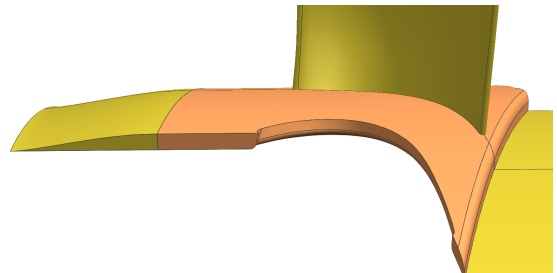


FIGURE 1: The turbine facility sketch.



(a) Flat insert without step.



(b) Flat insert with step.

FIGURE 2: Backward facing step.

fillet geometry was found after many CFD calculations and then it was tested. The authors achieved to eliminate the horseshoe vortex and observed a reduction in the passage vortex. Results also showed a decrease in the level of streamwise vorticity and turbulent kinetic energy. However, the authors did not mention about the secondary loss measurements.

Shih and Lin [5] carried out computational studies to see the effects of the leading edge fillets and the given inlet swirl on the secondary flows, losses related to these secondary flows and the surface heat transfer. Two different leading edge fillets were tested. One having zero thickness on the blade surface, and the other having zero thickness on the endwall. The authors claimed that both inlet swirl and leading edge fillets could reduce surface heat transfer (10% on the airfoil and 30% on the endwalls) and

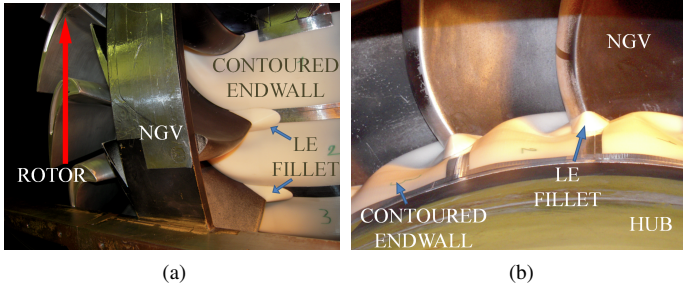


FIGURE 3: Experimental setup.

TABLE 1: The AFTRF design performance parameters.

Inlet Total Temperature ($^{\circ}\text{K}$); T_{0_1}	289
Inlet Total Pressure (kPa); P_{0_1}	101.36
Mass Flow Rate (kg/s); Q	11.05
Rotational speed (rpm); N	1300
Total Pressure Ratio; P_{0_1}/P_{0_3}	1.0778
Total Temperature Ratio; T_{0_3}/T_{0_1}	0.981
Pressure Drop (mmHg); $P_{0_1} - P_{0_3}$	56.04
Power (kW); P	60.6

the aerodynamic losses by more than 40% on its own. The authors concluded that even though the horseshoe vortices and the crossflows were not eliminated, the loss and the heat transfer coefficient were reduced, which implied that the reduction must be more complex than the intensity and the size of the secondary flows.

Lethander et al. [6] used an optimization program together with a CFD software to design an effective leading edge fillet in order to minimize the adiabatic wall temperature at the junction of the blade and the endwall. The results showed that the fillet hindered the formation of the horseshoe vortex, which in turn avoided the full development of the passage vortex. But, total pressure loss increased slightly. Nevertheless, the fillet was able to perform well in terms of thermal benefits. The reduction in the secondary flows prevented the cooler near-wall fluid to lift off from the endwall and the fillet surface.

Becz et al. [7] performed wind tunnel tests using Sauer et al.'s [3] two bulb like geometries and a leading edge fillet to compare them with the baseline configuration. The design of Sauer et al. [3] was used to create these bulbs. The fillet had two boundary layer thickness in height and eight boundary layer thickness in length. Area averaged total pressure loss results at a downstream

TABLE 2: The AFTRF design features.

Rotor Hub Tip Ratio	0.7269
Tip Radius (m); R_{tip}	0.4582
Blade Height (m); h	0.1229
Tip Relative Mach Number	0.24 (max)
Nozzle Guide Vane (tip)	
number	23
chord (m)	0.1768
spacing (m)	0.1308
turning angle	70
maximum thickness (mm)	38.81
Midspan Axial Chord	
nozzle (m)	0.1123
rotor (m)	0.09294
Vane Reynolds Number	
based on inlet velocity	$(3 \sim 4) \times 10^5$
based on exit velocity	$(9 \sim 10) \times 10^5$

location showed that the large bulb geometry slightly increased the loss. On the other hand, small bulb and leading edge fillet reduced the loss by 8%. In the later paper of Becz et al. [8], authors carried out experiments on the small bulb and leading edge fillet. But this time, they showed the mass-flow averaged total pressure loss results. The reason was to take into account the effect of mass flux in order to calculate the entropy production correctly. Compared to the first paper [7], small bulb did not lessen the total pressure loss. The leading edge fillet geometry again showed a reduction in loss by an amount of 7.3%.

Mahmood et al. [9] experimentally investigated the effect of leading edge fillets on secondary flows and Nusselt Number in a linear blade passage. Four different types of fillets were tested, details of which are given in the paper. Based on flow visualizations, smaller horseshoe vortex occurred in front of the leading edge when compared to baseline. Total pressure loss coefficient results, measured at a downstream location, exhibited no reduction. The authors also noted that the passage vortex was shifted upwards.

Han and Goldstein [10] performed mass transfer experiments in a turbine cascade with a leading edge fillet. The leading edge fillet was designed in the same way as described in Zess an

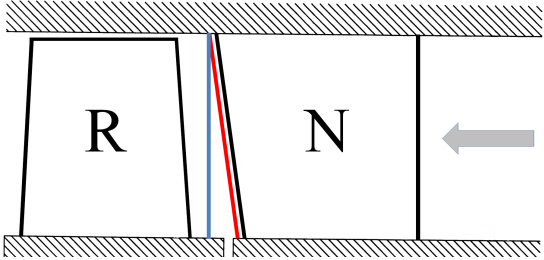


FIGURE 4: Rotor inlet plane perpendicular to axial direction and NGV exit plane parallel to NGV trailing edge.

Thole's paper [4] with modified dimensions. Low and high turbulence intensity flow conditions were tested. Both with the low and the high turbulence intensity measurements, the horseshoe vortex was reduced and the passage vortex was delayed. However, the strength of the passage vortex was found to be similar in magnitude to the baseline case near the trailing edge of the blade. Authors also noted that the fillet increased the leading edge corner vortices on the suction and pressure sides. Authors did not mention about the total pressure losses.

This paper includes the experimental investigation of the specific NGV leading edge fillets designed for the Axial Flow Turbine Research Facility (AFTRF). The aerodynamic performance of these fillets are experimentally tested on the cylindrical hub surface and also on a nonaxisymmetric contoured endwall designed by Turgut and Camci [11]. The following sections will give detailed information about the design methodology of these leading edge fillets. The aerodynamic experiments performed in this study are also supported by the computational fluid dynamics evaluation and the predictions are presented at the NGV exit.

EXPERIMENTAL FACILITY

The Axial Flow Turbine Research Facility (AFTRF) is installed at the Turbomachinery Aero-Heat Transfer Laboratory of the Pennsylvania State University. The AFTRF is a low speed, single-stage, cold flow turbine having a diameter of 91.66cm. Table 1 summarizes the design performance parameters of the turbine facility and the features are shown in Tab. 2. The detailed description and the characteristics of the AFTRF can be found from [12–15]. The facility is driven by four axial suction fans downstream of the rotor section and the speed of the rotor is controlled by a power absorbing eddy-current brake. Inlet has a bell-mouth shape followed by the NGV row and the rotor blades. A sketch of the AFTRF is given in Fig. 1. There are 23 NGV's and 29 rotor blades followed by the exit guide vanes.

In order to test performance of the contoured endwall and the leading edge fillet designs with a reference baseline, "Flat In-

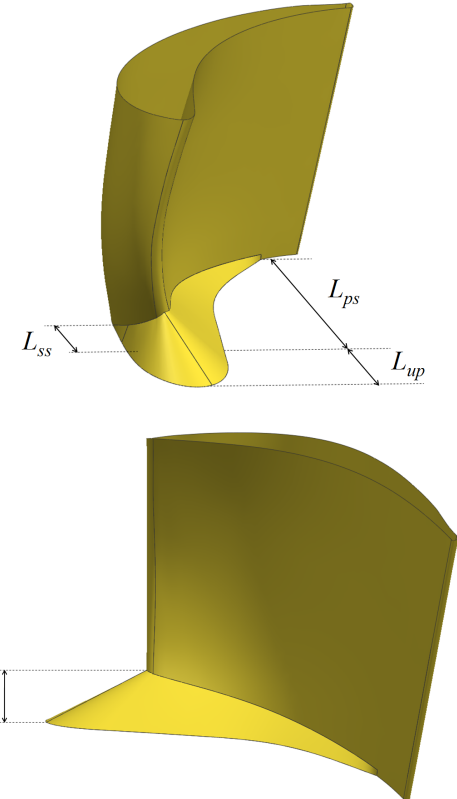


FIGURE 5: Leading edge fillet design characteristic length definitions.

sert" is manufactured using stereolithography (SLA) technique. This Flat Insert has cylindrical endwall surface in the vane passage and has a thickness of 0.0075m, corresponding to ~6.1% of the vane span. It extends one midspan axial chord of the vane in upstream direction. It has a linear ramp with rounded edges to maintain surface continuity. Flat Insert ends at the rim seal with a backward facing step. The solid model of this insert is shown in Fig. 2. The effect of backward facing step will be investigated computationally in the following sections.

The complete stage of the AFTRF is shown in Fig. 3a. In this picture, the SLA parts of contoured endwall and one of the leading edge fillet designs are also installed in the NGV row. Figure 3b shows a view of the NGV row and the SLA parts from the upstream of the leading edge. Note that, 0.05mm (2 mils) thick aluminum tape is used for the continuity between the surfaces. SLA parts are attached to the hub surface with double-sided tape.

The blue vertical line in Fig. 4 indicates the experimental measurement plane. This axial plane is located at $x/c = 1.018$ from the NGV trailing edge at casing. The radial starting location for the measurements is selected as the %8 of the vane. The reason is that the thicknesses of SLA parts downstream of the trailing edge are %6.1 of the vane span. It is also found out

TABLE 3: Leading edge fillet design features.

	H	L_{up}	L_{ps}	L_{ss}
	% Span	% c_{hub}	% c_{hub}	% c_{hub}
F02linear	0.08	0.27	0.28	0.22
F03curved	0.15	0.37	0.88	0.33
F03linear	0.15	0.37	0.88	0.33
F04curved	0.15	0.37	0.98	0.33
FC02linear	0.08	0.27	0.28	0.22
FC03curved	0.15	0.37	0.88	0.33
FC03linear	0.15	0.37	0.88	0.33
FC04curved	0.15	0.37	0.98	0.33

that above %35 of the span, the variations in measurements are minimal. Therefore, the maximum location in radial direction is selected as %38 of the span, which helped in reducing the time needed for a complete measurement of one pitch in circumferential direction.

The total pressure measurements are carried out by a Kiel probe manufactured by United Sensor Corporation [16]. The probe has a 3.175mm (0.125in.) head diameter. The main advantage of Kiel probe is the extensive range of insensitivity to yaw and pitch angles. The manufacturer documents the ranges as $\pm 48^\circ$ and $\pm 45^\circ$ for yaw and pitch, respectively. Before the experiments, probe is manually aligned with the NGV exit flow design angle, which is 70° from the axial direction. Zaccaria and Lakshminarayana [12] reported that the flow yaw and pitch angles deviate from design value within $\pm 5^\circ$. The probe is mounted on a single-axis linear traverser which moves in radial direction. This linear traverser is installed on a circumferential traverser that is attached to the facility window. The slot on the window allows the circumferential traversing mechanism to complete 1.5 vane pitch. But, authors decided to traverse one full pitch in circumferential direction for time considerations. There are 18 radial and 25 circumferential locations that the probe collects data, which makes 450 data points.

Kiel probe is connected to a pressure transducer, and the analog data from the transducer is transferred to a 12 bit data acquisition (DAQ) board. A computer program is developed using commercial software LabView which reads the data coming from DAQ and performs necessary calculations and exports the C_{Pr} values. The estimated uncertainty in C_{Pr} is 0.6%.

DESIGN METHODOLOGY

Nonaxisymmetric Endwall Contouring

Nonaxisymmetric endwall contouring is accomplished by two steps. First step is to define splines within the vane passage at various axial locations. These splines are in the form of Fourier series expansion. First three terms of the Fourier series is found to be sufficient to create highly complex circumferential curve. Secondly, these splines are imported by a solid modeling software, in which they are combined to form a three-dimensional contoured endwall. The detailed description of the endwall contouring design is given in the previous paper of Turgut and Camci [11]. In that paper, various contoured endwalls were presented and computationally evaluated. Among all the designs, case D14 was found to be promising. So that, it will be tested experimentally to see its influence on the total pressure distribution.

Leading Edge Fillet Design

The mechanism of the horseshoe vortex formation and the separation into two parts is not the same for all turbine blades. According to Langston [17], the separation at the saddle point depends on the blade surface pressure distribution rather than the leading edge shape. So, a particular leading edge fillet should be designed for each turbine blades depending on the pressure field. But, there are some certain conventions while designing the fillet. Sung and Lin [18] suggested to design the fillet such that its length is greater than the height. Also, they proposed the height to be at least one boundary layer thickness for symmetric airfoils. Zess and Thole [4] tried various configurations of height to length ratio. They also examined the fillet profile and decided on using a fillet with a linear slope.

The current LE fillet designs are based on the discussions mentioned above. Figure 5 describes the LE fillet design parameters. H represents the height of the fillet in the radial direction from the cylindrical endwall based on the vane span; L_{up} , L_{ps} , and L_{ss} are the distances from leading edge, in terms of axial chord length at hub, showing to what extent fillet is designed in upstream axial direction, along pressure and suction surfaces, respectively. In the present study, four different types of LE fillet are introduced. Two of them have a linear cross-section, and the other two have a parabolic cross-section. The linear ones are named as “F02linear, F03linear”, and the ones with parabolic profiles are named as “F03curved, F04curved”. These four LE fillets are designed in such a way that they are placed on a cylindrical endwall. Moreover, the performance of these fillets are also investigated on the contoured endwall, namely “FC02linear, FC03linear, FC03curved, FC04curved”. Table 3 lists the design parameters for all these designs. In addition to this, Fig. 6 illustrates the solid model representation of LE fillets. In this figure, the Flat Insert and the LE fillets sitting on cylindrical endwall are in the left two columns; the contoured endwall and the LE fillets designed for contoured endwall are in the right two columns.

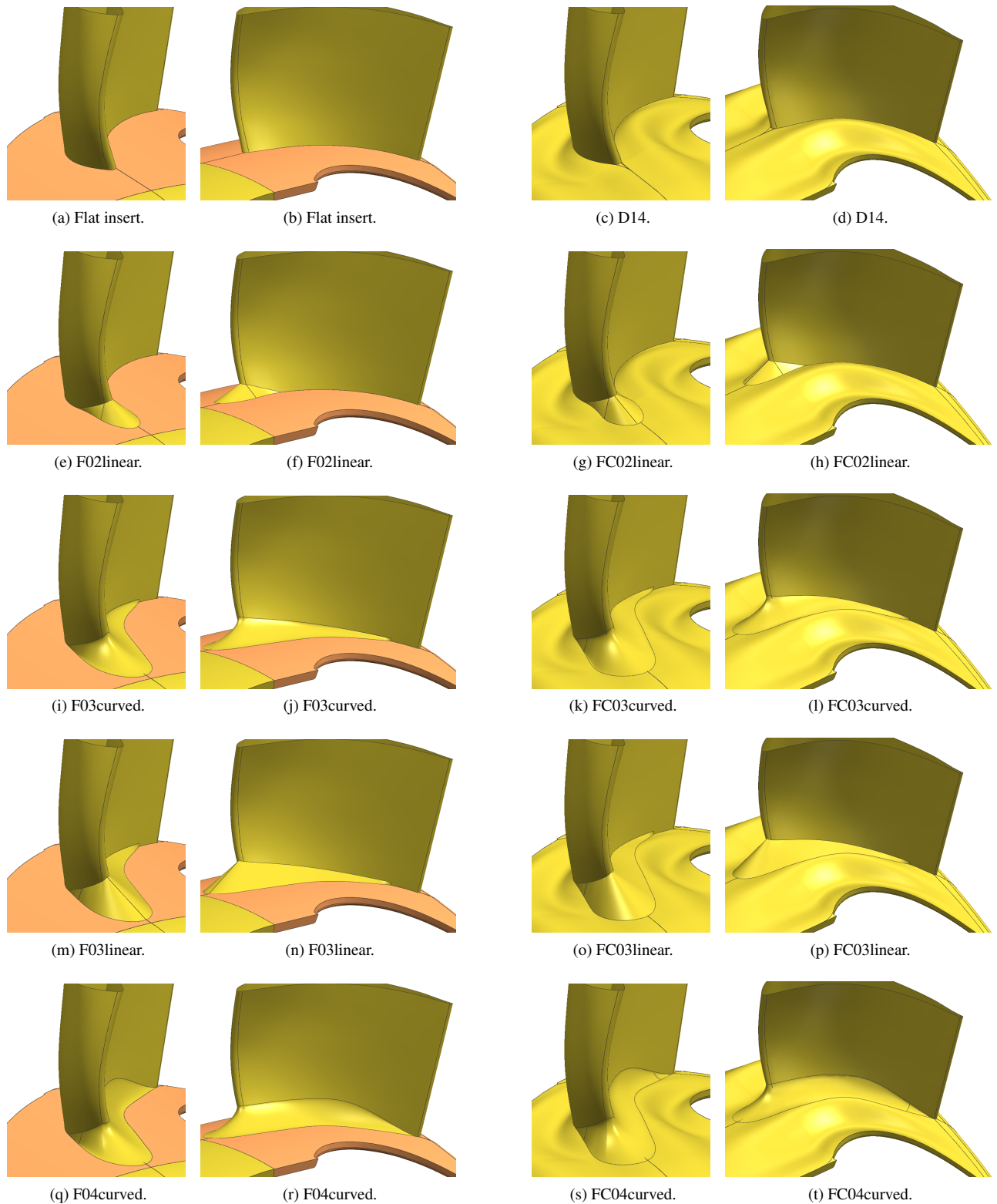


FIGURE 6: Leading edge fillet designs.

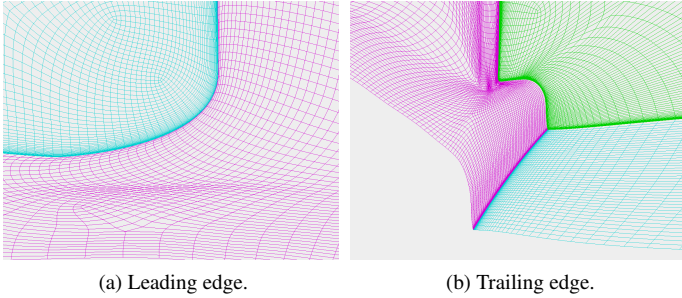


FIGURE 7: Structured grid.

F02linear and FC02linear have a design such that L_{up} is approximately twice the length as H . The remaining LE fillets have more aggressive designs which doubled the height of the fillet and extend on the pressure side and hub intersection. F03 designs elongates on the pressure side as far as $c_{hub} = 0.88$, whereas F04 designs reaches to the $c_{hub} = 0.98$ point with more filling effect on the pressure side and hub intersection corner.

COMPUTATIONAL DETAILS

The computational evaluations of the nonaxisymmetric end-walls and leading edge fillets are accomplished by the commercially available finite-volume flow solver ANSYS CFX. The steady-state, three-dimensional flow simulations are performed for an annular NGV passage, without including the rotor section.

The computational domain extends one midspan axial chord in the upstream direction, where the experimental inflow conditions are imposed. The circumferentially averaged total pressure and turbulence kinetic energy distribution along the span are specified at the inlet boundary according to the previous experimental research [15]. The outflow boundary is located two chords downstream of the NGV trailing edge and mass flow rate is set at the outlet. NGV, hub, and casing walls have no-slip boundaries with adiabatic conditions. Only one NGV passage is simulated with rotationally periodic side walls.

Menter's [19] two-equation eddy-viscosity model gives good predictions especially when there is an adverse pressure gradient in the boundary layer. This shear stress transport (SST) model is based on $k-\omega$ turbulence closure formulation. Also, the flow through an NGV passage is transitional, and one should account for the transition effects as discussed in [20]. One of the methods to predict the transition is the Gamma Theta model in CFX. This model is based on an empirical correlation and two more transport equations are solved; one for the momentum thickness Reynolds number (Re_{θ_l}), and the other for the intermittency (γ). This model is validated for various transitional flows together with SST turbulence model.

Based on the discussion and the results presented in [20], the authors applied structured mesh to represent the flow field.

Three-dimensional computational mesh is created by GRIDPRO. Multi-block, body-fitted structured grid gives more reasonable flow predictions in comparison to unstructured grid, even though unstructured mesh is easy and quicker to implement for complex geometrical designs. An example of a generated structured grid is shown in Fig. 7. This figure shows leading edge and trailing edge view of FC04curved design. Note that, in the trailing edge view, there is an axial plane included to demonstrate how the backward facing step is handled. The structured grid is well adapted to the endwall contouring, leading edge fillet and the backward facing step. Since the near-wall grid resolution is the key for transitional flows and for capturing the secondary flow formation, the non-dimensional wall distance of $y^+ < 1$ is satisfied everywhere in the domain. Total number of 2 million three-dimensional mesh elements are used in the computational domain. This mesh density gives grid independent results, especially on the total pressure coefficient distribution at the NGV exit.

The computational evaluation of the designs are performed on two planes. One is the rotor inlet plane where the experimental measurements were taken. The other plane is parallel to the NGV trailing edge, located at $x/c = 1.025$ away from the trailing edge line. These planes are shown in Fig. 4.

RESULTS AND DISCUSSION

Backward Facing Step

As mentioned in the previous sections, Flat Insert is employed as a reference endwall for the evaluation of new designs. The Flat Insert, which is installed on the AFTRF, extends up to the end of NGV row and it has a backward facing step as was shown in Fig. 2b. This had to be fabricated that way because of the physical limitations of the facility. But still, it is important to analyze the fluid flow structures behind this backward facing step. In order to isolate its effects, a new solid model of Flat Insert is completed without having a step, as was shown in Fig. 2a. This model is designed for computational assessment. After the NGV trailing edge, the cylindrical endwall extends to the outflow boundary of the domain, which lies two c downstream.

The consequence of the backward facing step is investigated both at the NGV exit plane and the rotor inlet plane. Contours of C_{P_l} at NGV exit plane tells that the main difference between these two cases is the location of the secondary flow core, as shown in Fig. 8. For the Flat Insert with step case, the core is closer to the endwall. The reason is that the radial velocity component of the flow near the endwall increases after the step, and hence, there occurs a downward moving of the flow in radial direction. This influences the upstream also, and the secondary region is pulled towards the endwall.

Figure 9 shows the C_{P_l} contours at the rotor inlet plane, after the backward facing step. It should be pointed out that the reference constant y lines in Fig. 9 are not the same as the ones

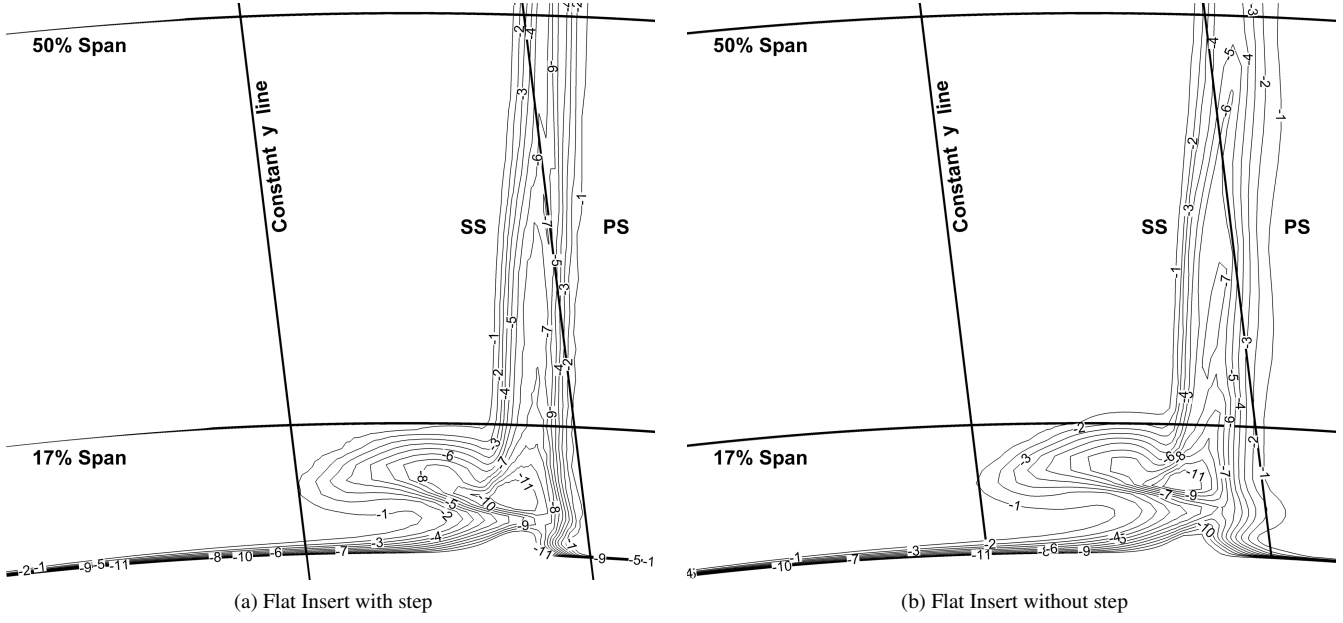


FIGURE 8: Contours of C_{P_t} at NGV exit plane, computational result.

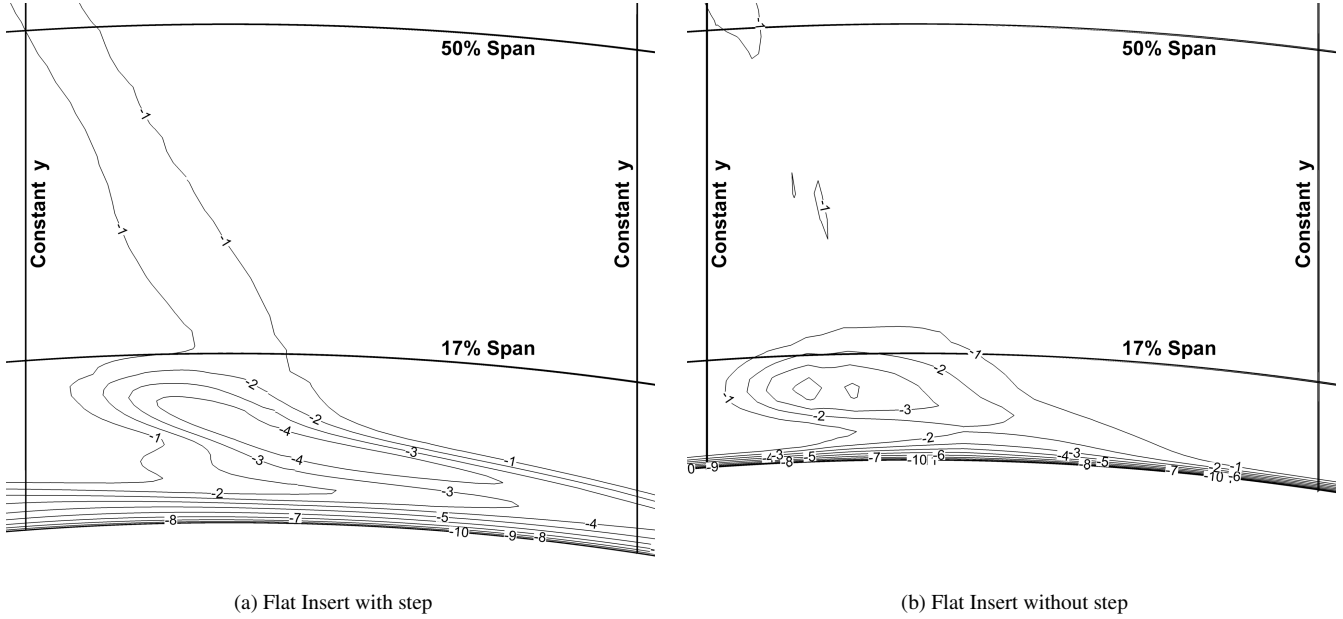
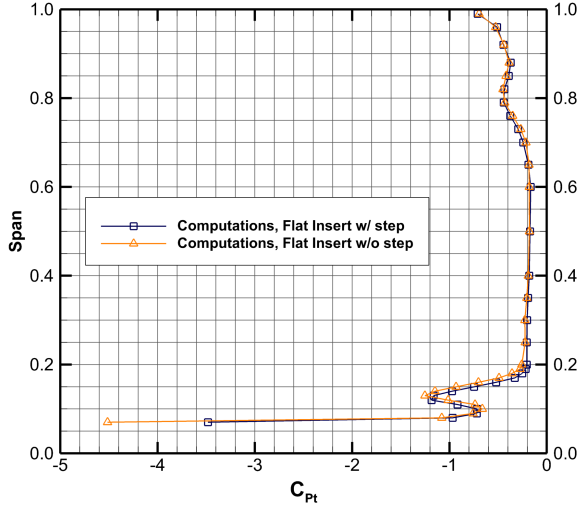


FIGURE 9: Contours of C_{P_t} at rotor inlet plane, computational result.

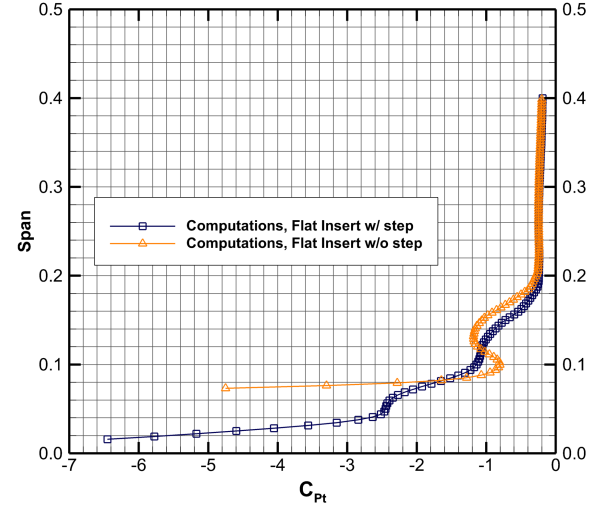
in Fig. 8. Also, as a reminder, the hub endwall for Flat Insert without step starts around 6% span. It is clear from this figure that the upper edge of the secondary flow area remains almost at the same radial position for both cases. Another important observation is the minimum value of C_{P_t} decreases to -4 for both cases. The contour plot for Flat Insert with step reveals that the secondary flow area is diffused to the endwall after the step. On

the other hand, Flat Insert without step has the secondary flow area more concentrated at a region. The wake is spread out for the case without step.

The circumferentially mass flow averaged C_{P_t} distributions along the span for NGV exit plane and rotor inlet plane are shown in Figs. 10a and 10b, respectively. As discussed previously, there is a radially outward shift of approximately 1% span in the C_{P_t}



(a) NGV exit plane



(b) Rotor inlet plane

FIGURE 10: Effect of backward facing step on C_{P_t} distribution, computational result.

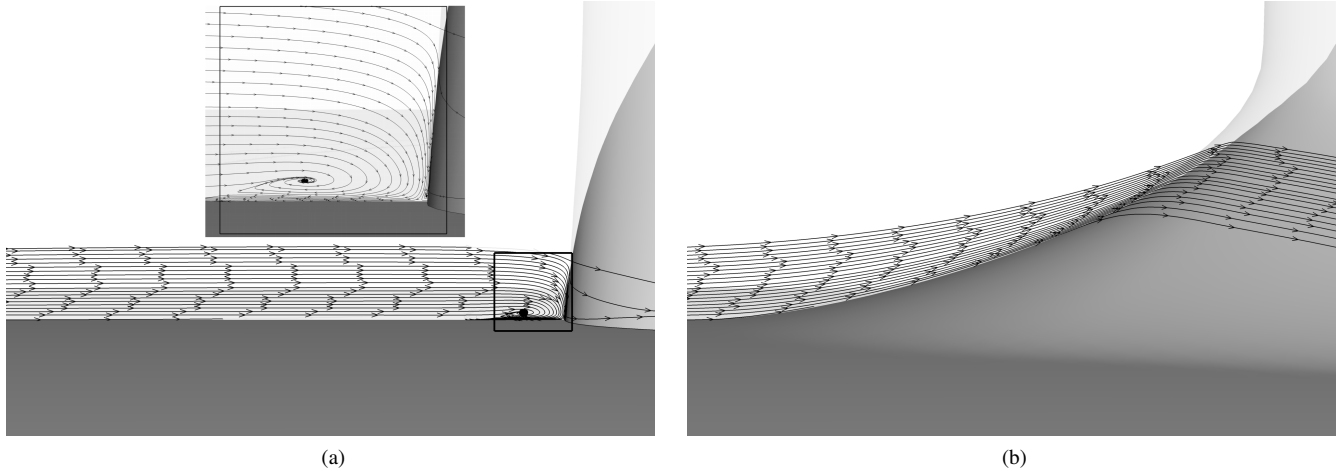


FIGURE 11: Effect of leading edge fillet on horseshoe vortex formation.

distribution, at the NGV exit plane. The comparison in Fig. 10a tells that the distributions do not change after 25% span.

The story behind the step is little different. The distribution for the case without step has a secondary flow more concentrated in a region, which is in accordance with Fig. 9b. On the other hand, there are two kinks in C_{P_t} distribution of the case with backward facing step, as shown in Fig. 10b. One is around 12% span, and the other one is near 6% span. The first one is related to the secondary flow and it is closer to the endwall by 1% span compared to the Flat Insert without step. This result is similar to Fig. 10a. The second kink occurs since there is a diffusion of the secondary flow after the step.

Effect of Leading Edge Fillet

The purpose of using LE fillets were to minimize the horseshoe vortex formation. Figure 11 depicts how efficiently the LE fillet works. The Flat Insert endwall and LE junction is shown in Fig. 11a. A circumferential plane, extending from the leading edge in the upstream direction, is extracted and the streamlines are released on this plane. The horseshoe vortex is captured within the 5% of vane span, and it is magnified for a better resolution. This horseshoe vortex is completely eliminated with the use of LE fillet as shown in Fig. 11b. For both figures, the circumferential planes and the streamlines are the same. Since the flow does not meet the leading edge with a sharp corner at the hub, streamlines climb up the ramp and follow the fillet geom-

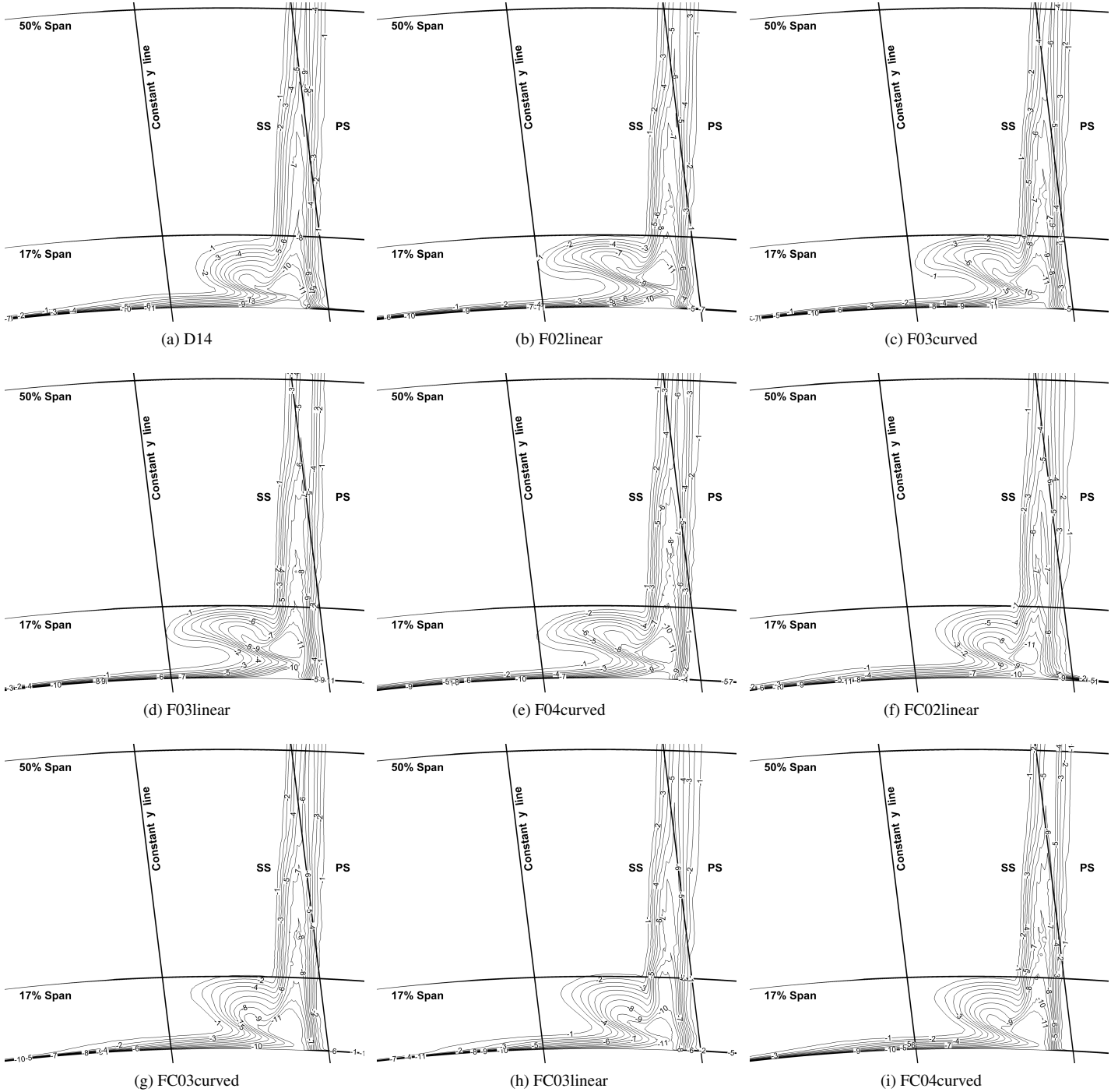
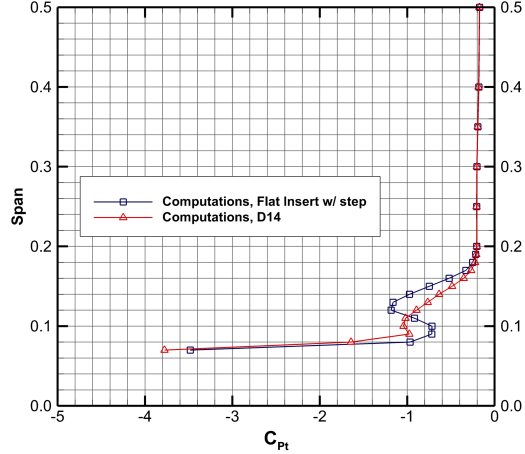


FIGURE 12: Computational C_p contours at NGV exit plane.

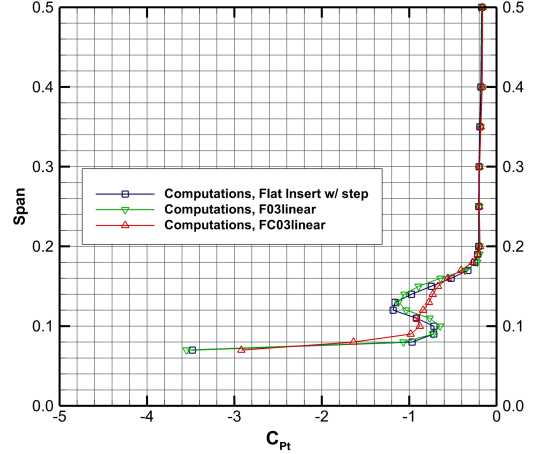
try nicely. The further details of the results with LE fillets will be examined at NGV exit plane and rotor inlet plane in the following sections.

Contoured Endwall and Leading Edge Fillet Designs

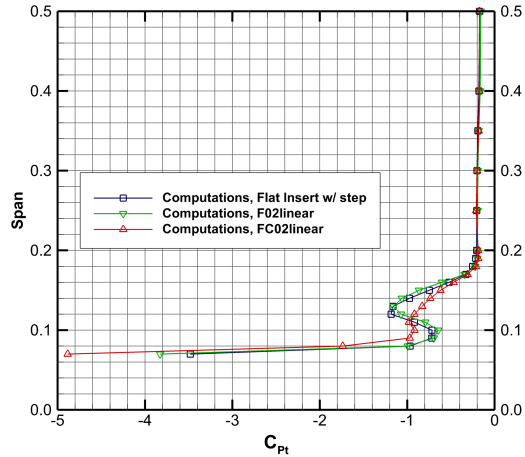
Four different LE fillet designs are evaluated both computationally and experimentally. These fillets are attached to the Flat Insert as well as the contoured endwall. The aim is to see



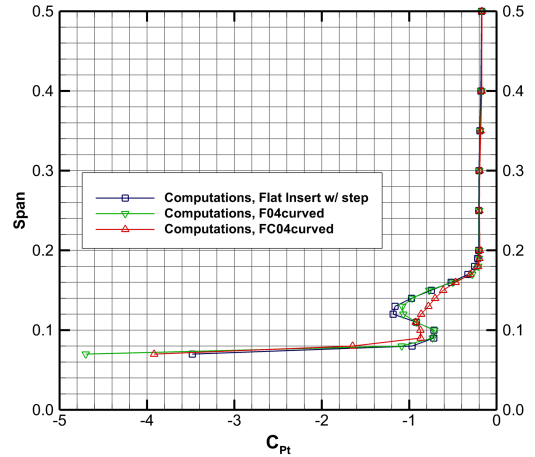
(a) D14



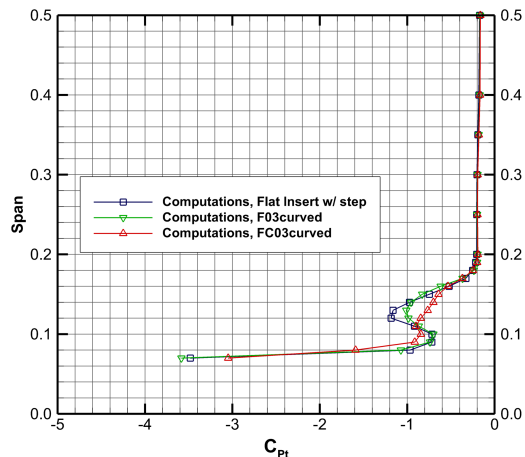
(a) F03linear and FC03linear



(b) F02linear and FC02linear



(b) F04curved and FC04curved



(c) F03curved and FC03curved

FIGURE 13: Computational C_{P_t} distributions along the span at NGV exit plane.

the individual behavior of the fillets on a cylindrical endwall surface, and also, to analyze the performance of these designs in combination with the contoured endwall. As discussed earlier, there are two planes that the results will be compared, namely the NGV exit plane and the rotor inlet plane.

Equal contour lines of C_{P_t} at NGV exit plane are shown in Fig. 12. The same constant y lines in Fig. 8 are used to form a basis for comparison. The first thing that is apparent is the contoured endwall itself and the combination of LE fillets with contoured endwall result in a smaller secondary flow area. On the contrary to this favorable result, contouring the endwall increases the total pressure loss just above the endwall. For instance, at a constant y location, the thickness of the total pressure loss contours reach up to 8.3% of the span for contoured endwall case

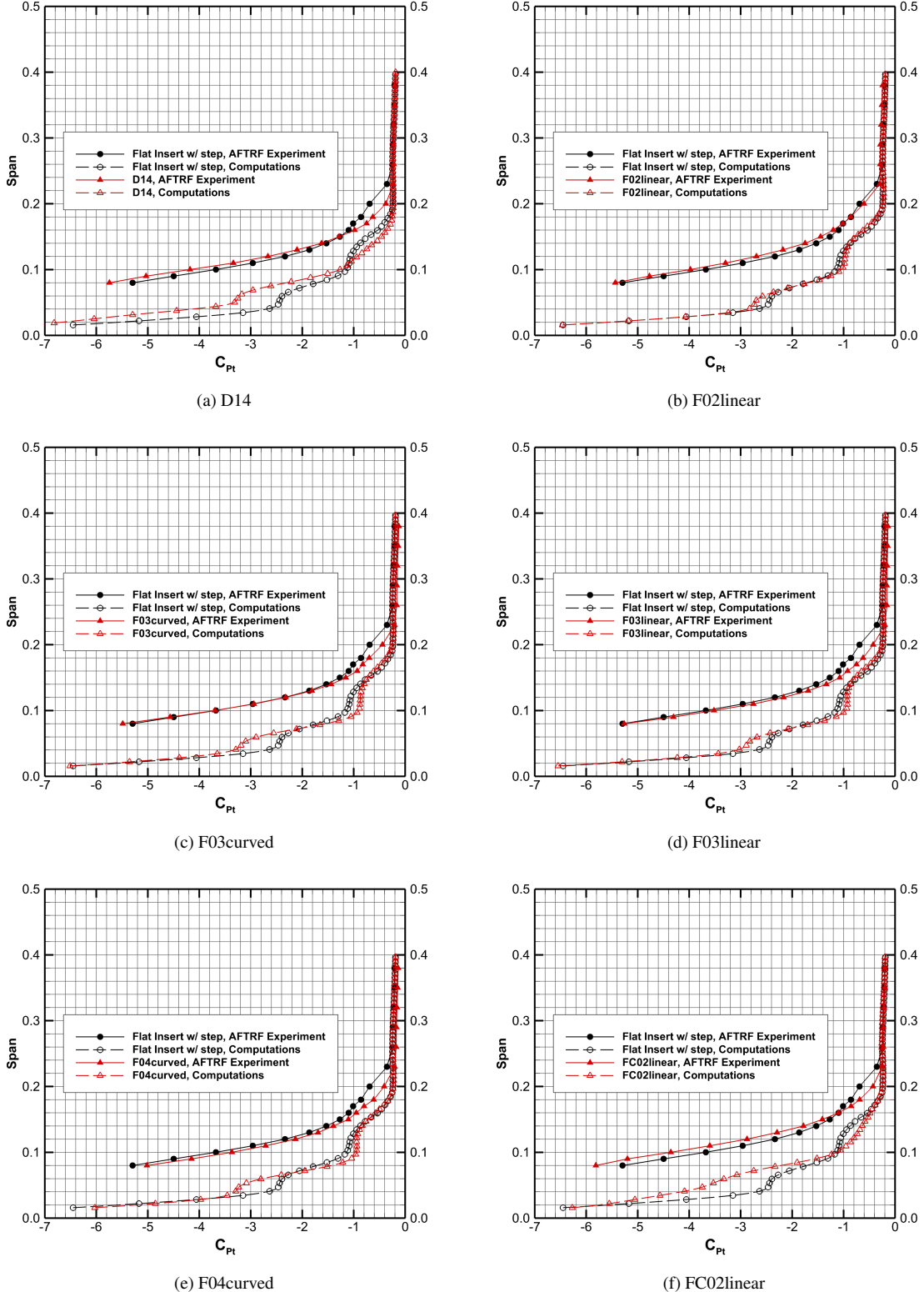


FIGURE 14: Circumferentially area-averaged C_{Pt} distribution along the span at rotor inlet plane.

D14, as shown in Fig. 12a. Whereas, for F03linear in Fig. 12d, the thickness of the contour lines at the same y location is around 7.5% span.

The more quantifiable discussion can be achieved from the circumferential mass flow averaged values. Figure 13 shows the comparison between the reference Flat Insert case and contoured endwall and LE fillet cases at the NGV exit plane. The sole effect of contoured endwall case, D14, is analyzed in Fig. 13a. Clearly, case D14 changes the C_{Pt} distribution considerably. From 12% to 18% span, the circumferentially mass flow averaged values are reduced compared to Flat Insert case. The reduction reaches 33% of C_{Pt} at 13% span. Conversely, from 11% span to the endwall, the total pressure loss is increased. This is mainly due to the fact that the valley on the endwall near the suction surface pulls the secondary flow loss region to the hub endwall. That results in higher values of C_{Pt} near the endwall.

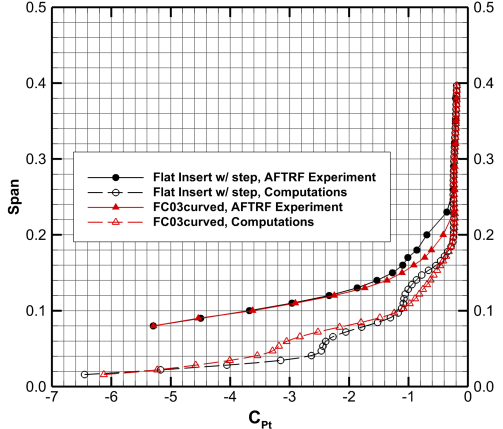
It is observed from Fig. 13b that the F02linear reduced the mass flow averaged values from 10% to 13% span, but then increased from 14% to 17%. There is a slight radially outward shift in the distribution, approximately 0.5% span. The combination of contoured endwall and LE fillet, FC02linear, has a similar trend close to D14. From 16% to 12% span, C_{Pt} is less than those of Flat Insert, and the maximum reduction is around 30% of C_{Pt} .

F03curved reduced total pressure loss between 11% to 13% span, having a maximum reduction of 17% C_{Pt} value, as shown in Fig. 13c. FC03curved improved the loss distribution just above the endwall, 6.5% span, when compared to D14 in Fig. 13a.

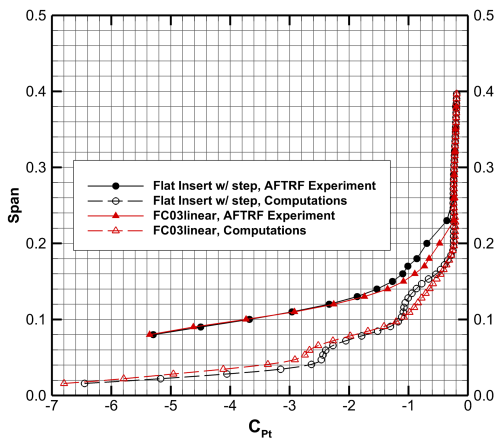
FC03linear in Fig. 13a has a very similar distribution to that of FC03curved. The total pressure loss is decreased 11% to 16% span with a maximum reduction of 33% C_{Pt} . And, it is increased between 11% to 8% span. Again, the fillet attached to contoured endwall works effectively close to the hub endwall. It is seen from this figure that FC03curved has shifted the profile 0.6% span in the radially outward direction, between 11% and 18% span locations.

F04curved is the design extending on the pressure surface to the trailing edge corner. It covers larger area at the corner of pressure surface and hub endwall. It decreased the peak value of C_{Pt} by 12% around 12% span. However, the loss is increased 34% very close to the hub endwall. FC04curved has a similar distribution to that of FC03curved.

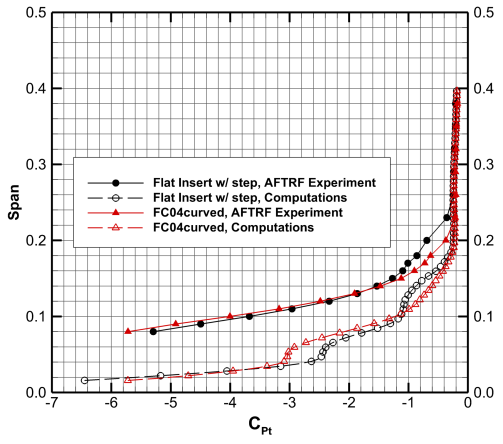
The authors of this paper performed the experiments at the rotor inlet plane. The area-averaged total pressure coefficient distributions are plotted in Fig. 14. The solid lines represent the experimental data, whereas the dashed lines display computational simulation results. Before going into detailed discussion of these figures, it is required to mention one observation. There is an obvious disagreement between the experimental and computational distribution, particularly below 23% span. The wake C_{Pt} values are predicted well, but the discrepancy starts at the secondary flow area. The deviation of the CFD simulation from the



(g) FC03curved



(h) FC03linear



(i) FC04curved

FIGURE 14: Circumferentially area-averaged C_{Pt} distribution along the span at rotor inlet plane (Continued).

measurement has two main reasons:

- Rotor-vane interaction is not included in the simulation. Computations are carried on without the rotor geometry, only the vane is simulated.
- There is a radially outward flow through the rim seal caused by centrifugal force due to the rotation of the rotor section. The CFD calculation does not involve this flow.

It is expected that including these important considerations will improve the computational estimations. So, it is crucial that when discussing the current results, these factors should be kept in mind.

Apparently, at the rotor inlet plane, the secondary flow region in Fig. 14 is not as distinct as in Fig 13. The endwall boundary layer loss and secondary flow loss are combined. However, from Flat Insert experimental distribution in Fig. 14a, it can be said that the secondary flow starts around 26% span. Based on this information, experimental measurement shows that D14 reduced the loss up to 44%. But, below 15% span it increases the loss. CFD simulation predicts in the same trend, the secondary flow in D14 is less than Flat Insert, and loss is higher near the endwall. This is in accordance with the discussion for the results at NGV exit plane. Both the experimental and computational assessment tell that the secondary loss core is more closer to the endwall and the secondary flow region is diffused along the vane pitch near the endwall.

F02linear experimental distribution has 14% improvement on secondary flow, as shown in Fig. 14b, however, below 17% span the C_{P_t} is higher than Flat Insert values, as much as 19%. CFD estimates 11% reduction in secondary flow loss, and 12% increase in endwall boundary layer loss.

For F03curved case shown in Fig. 14c, measured loss is less than the Flat Insert between 26% and 14% span. Below that point C_{P_t} values are close to each other, except at 8% span, where the loss is measured 4% more than the reference value. The computational simulation successfully estimated the loss reduction in secondary flow region, but on the other hand, it calculated a 30% increase in loss closer to the endwall.

F03linear and F04curved showed improvement in loss recovery from 26% to 8% span as shown in Figs. 14d and 14e, respectively. CFD predicts the loss recovery in secondary flow area, however, there is an increase in loss below that region. This is a common prediction in all design simulations. But note that, F04curved has a positive influence within the endwall boundary layer, which is consistent with the experimental data.

The distribution for FC02linear is similar to that of D14, as shown in Fig. 14f. There is a gain in total pressure loss between 26% and 16% span, and an increase in loss below that radial location. Consistently, CFD predicts a reduction in secondary flow, and rise in C_{P_t} values near endwall.

Figures 14g and 14h depict the C_{P_t} distribution for the cases FC03curved and FC03linear, respectively. Both experimental

TABLE 4: Measured and computed percent change in C_{P_t} at the rotor inlet plane.

	Experiment	CFD	CFD
	Area-Av.	Area-Av.	Mass-Av.
D14	-1.08	6.77	6.01
F02linear	-7.95	1.62	2.10
F03curved	9.38	7.38	6.92
F03linear	14.10	3.37	3.37
F04curved	15.06	6.95	6.20
FC02linear	-7.07	3.43	1.64
FC03curved	9.18	6.35	5.70
FC03linear	7.43	6.99	6.26
FC04curved	4.28	6.58	5.57

TABLE 5: Computed percent change in C_{P_t} at the NGV exit plane.

CFD Mass Flow Averaged	
D14	0.31
F02linear	1.31
F03curved	0.49
F03linear	0.36
F04curved	-1.05
FC02linear	-0.54
FC03curved	1.84
FC03linear	1.80
FC04curved	0.73

measurements show that the secondary flow loss is reduced, without any increase in C_{P_t} near 8% span. On the other hand, FC04curved, shown in Fig. 14i, has a negative effect below 13% span. However, like the other designs, it decreased the secondary flow loss values. The numerical estimation of these three designs have similar pattern, except below the secondary flow region. FC04curved has lowered the loss generation in the endwall boundary layer up to 11%.

Table 4 lists the percent change in C_{P_t} at the rotor inlet plane. Remember that, the averaging is completed between 8% to 38% span for one pitch. Area-averaged experimental measurements tell that the most efficient designs are F03linear and F04curved with percent change values of 14.10 and 15.06, respectively. Besides, area-averaged percent change in CFD calculation for these designs are 3.37 for F03linear, and 6.95 for F04curved. Note that, based on the CFD area-averaged values, LE fillet designs combined with contoured endwall have the most total pressure loss reduction, except the short LE fillet configuration, FC02linear. The short LE fillet geometries, namely F02linear and FC02linear, increased C_{P_t} in experimental measurements. This is in accordance with the numerical prediction.

The mass flow averaged C_{P_t} is calculated at the NGV exit plane also, and the percent changes with respect to Flat Insert are listed in Tab. 5. Note that, this mass flow averaging is obtained over the whole NGV passage exit. The most promising results come from FC03curved and FC03linear with percent change values of 1.84 and 1.80, respectively.

CONCLUSIONS

Four different LE fillets were designed for the NGV of the low-speed turbine rig, AFTRF. The performance of these LE fillets and a contoured endwall were tested experimentally and computationally. Numerical evaluation was achieved without the rotor simulation. A reference baseline, Flat Insert, with constant thickness and having cylindrical surface was used. Two sets of LE fillets were manufactured using SLA technique. First set was put on the Flat Insert, and the other set was sitting on the contoured endwall, D14.

The Flat Insert, which was located in NGV passage, extended from one midspan chord upstream of LE to downstream of TE where the NGV row ended. Therefore, it had a backward facing step. To distinguish the influence of this step, a computational assessment study was accomplished with and without backward facing step. The comparison showed that the C_{P_t} distribution is 1% closer to the endwall in the case with backward facing step. The loss is diffused after the step.

LE fillets managed to remove the horseshoe vortex occurring in front of the LE. In one of the LE fillet cases sitting on Flat Insert, CFD results at the NGV exit showed that the mass-averaged loss value was reduced 1.31% for the whole passage exit. One of the LE fillets increased the loss at NGV exit. At the rotor inlet plane, the experimental measurements were taken between 8% and 38% span. The area-averaged loss values showed different trend. The most efficient one turned out to increase the loss after the backward step. The other three designs decreased the area-averaged loss with the maximum reduction of 15.06%. CFD estimated that all designs reduced the area-averaged C_{P_t} up to 7.38%.

Contoured endwall effectively weakened the secondary flow

region. Mass-averaged loss before the step at NGV exit was reduced by 0.31%. However, area-averaged experimental measurement showed that it increased the loss at rotor inlet plane, although CFD calculated 6.77% decrease.

The combination of contoured endwall and LE fillets were tested also. Before the step, three of the designs worked well and the loss was estimated less than Flat Insert up to 1.84%. The rotor inlet plane experiments confirmed this estimation. The same design had 9.18% reduction in area-averaged loss. CFD at this plane calculated as 6.35% reduction.

It should be noted that, not all the CFD evaluations are in accordance with the experimental measurements. Authors concludes that this has two reasons. One of them is the flow coming radially out from the rim seal. It is not simulated in the present paper. Another important issue is the rotor-vane interaction. Rotor is not included in the CFD. In the future work, the CFD validation of baseline NGV and rotor will be performed.

ACKNOWLEDGMENT

The authors acknowledge the financial support provided by the Siemens Energy Inc. and thank to Dr. Matthew Montgomery, Dr. Prakash Chander, Dr. Michael Crawford, Andrew Lohaus, Anthony Malandra, Ching-Pang Lee, Boris Dobrzynski, Humberto Zuniga, Ken Landis, and Dirk Nuernberger. The authors are thankful to Dr. Ali Aktürk for his support during this study. The authors are also indebted to Dr. Peter R. Eiseman of Program Development Company, LLC for his great help in grid development for our study.

REFERENCES

- [1] Sharma, O. P., and Butler, T. L., 1987. "Predictions of Endwall Losses and Secondary Flows in Axial Flow Turbine Cascades". *ASME Journal of Turbomachinery*, **109**, pp. 229–236.
- [2] Denton, J. D., 1993. "Loss Mechanisms in Turbomachines". *ASME Journal of Turbomachinery*, **115**, pp. 621–650.
- [3] Sauer, H., Müller, R., and Vogeler, K., 2001. "Reduction of Secondary Flow Losses in Turbine Cascades by Leading Edge Modifications at the Endwall". *ASME Journal of Turbomachinery*, **123**, pp. 207–213.
- [4] Zess, G. A., and Thole, K. A., 2002. "Computational Design and Experimental Evaluation of Using a Leading Edge Fillet on a Gas Turbine Vane". *ASME Journal of Turbomachinery*, **124**, pp. 167–175.
- [5] Shih, T. I.-P., and Lin, Y.-L., 2003. "Controlling Secondary-Flow Structure by Leading-Edge Airfoil Fillet and Inlet Swirl to Reduce Aerodynamic Loss and Surface Heat Transfer". *ASME Journal of Turbomachinery*, **125**, pp. 48–56.

- [6] Lethander, A. T., Thole, K. A., Zess, G., and Wagner, J., 2004. "Vane-Endwall Junction Optimization to Reduce Turbine Vane Passage Adiabatic Wall Temperatures". *Journal of Propulsion and Power*, **20**, pp. 1105–1116.
- [7] Becz, S., Majewski, M. S., and Langston, L. S., 2003. "Leading Edge Modification Effects on Turbine Cascade Endwall Loss". *ASME Paper No. GT2003-38898*.
- [8] Becz, S., Majewski, M. S., and Langston, L. S., 2004. "An Experimental Investigation of Contoured Leading Edges for Secondary Flow Loss Reduction". *ASME Paper No. GT2004-53964*.
- [9] Mahmood, G. I., Gustafson, R., and Acharya, S., 2005. "Experimental Investigation of Flow Structure and Nusselt Number in a Low-Speed Linear Blade Passage With and Without Leading-Edge Fillets". *ASME Journal of Heat Transfer*, **127**, pp. 499–512.
- [10] Han, S., and Goldstein, R. J., 2006. "Influence of Blade Leading Edge Geometry on Turbine Endwall Heat (Mass) Transfer". *ASME Journal of Turbomachinery*, **128**, pp. 798–813.
- [11] Turgut, Ö. H., and Camci, C., 2011. "A Nonaxisymmetric Endwall Design Methodology for Turbine Nozzle Guide Vanes and Its Computational Fluid Dynamics Evaluation". *ASME Paper No. IMECE2011-64362*.
- [12] Zaccaria, M., and Lakshminarayana, B., 1995. "Investigation of Three-Dimensional Flowfield at the Exit of a Turbine Nozzle". *Journal of Propulsion and Power*, **11**(1), January–February, pp. 55–63.
- [13] Lakshminarayana, B., Camci, C., Halliwell, I., and Zaccaria, M., 1996. "Design and Development of a Turbine Research Facility to Study Rotor-Stator Interaction Effects". *International Journal of Turbo and Jet Engines*, **13**, pp. 155–172.
- [14] Camci, C., 2004. "Experimental and Computational Methodology for Turbine Tip De-sensitization". *VKI Lecture Series 2004-02*, Turbine Blade Tip Design and Tip Clearance Treatment.
- [15] Zaccaria, M. A., 1994. "An Experimental Investigation Into the Steady and Unsteady Flow Field in an Axial Flow Turbine". PhD Thesis, The Pennsylvania State University, University Park, PA.
- [16] United Sensor Corporation, Kiel Probes. URL: <http://www.unitedsensorcorp.com/kiel.html>.
- [17] Langston, L. S., 2001. "Secondary Flows in Axial Turbines-A Review". *Heat Transfer in Gas Turbine Systems, Annals of the New York Academy of Sciences*, **934**, pp. 11–26.
- [18] Sung, C.-H., and Lin, C.-W., 1998. "Numerical Investigation on the Effect of Fairing on the Vortex Flows Around Airfoil/Flat-Plate Junctures". *AIAA Paper No. AIAA-88-0615*.
- [19] Menter, F. R., 1994. "Two-Equation Eddy-Viscosity Turbulence Models for Engineering Applications". *AIAA Journal*, **32**(8), pp. 1598–1605.
- [20] Turgut, Ö. H., and Camci, C., 2011. "A Computational Validation of Turbine Nozzle Guide Vane Aerodynamic Experiments in an HP Turbine Stage". *ASME Paper No. IMECE2011-64352*.